minerals

MDPI

Article

Petrogenesis and Tectonic Implications of the Ore-Associated Intrusions in Bayanbaolege Ag Polymetallic Deposit, Inner Mongolia, NE China

Xi Wang [1,2], Qun Yang [1,2,*], Zhen-Ming Sun [3] and Yun-Sheng Ren [1,4,*]

[1] College of Earth Sciences, Jilin University, Changchun 130061, China; xiwang@jlu.edu.cn
[2] Key Laboratory of Mineral Resources Evaluation in Northeast Asia, Ministry of Natural Resources of China, Changchun 130026, China
[3] Changchun Institute of Technology, Changchun 130012, China; sunzhenming.9040@163.com
[4] Institute of Disaster Prevention, Sanhe 065201, China
* Correspondence: yangqun@jlu.edu.cn (Q.Y.); renys@jlu.edu.cn (Y.-S.R.); Tel.: +86-131-5437-0506 (Q.Y.)

Abstract: The large Bayanbaolege Ag polymetallic ore deposit is located in the Tuquan-Linxi Fe (Sn)-Cu-Pb-Zn-Ag-Nb (Ta) polymetallic metallogenic belt, which is an important part of the Great Xing'an Range metallogenic province, northeast China. The sulfide–quartz vein-type orebodies in the deposit are mainly hosted in the Cretaceous granodiorite porphyry and Late Permian Linxi formation. The U-Pb dating of the zircon from the post-ore diorite porphyrite yields an age of 124.8 ± 1.1 Ma, which constrains the mineralization time at the Early Cretaceous. The Sr-Nd isotope values ($^{87}Sr/^{86}Sr)_i$ = 0.708576~0.710536; ε_{Nd} (t) = −0.51~+0.69; the Hf isotope values $^{176}Hf/^{177}Hf$ = 0.2827278~0.2830095, the ε_{Hf} (t) = +3.1~+11.2, T_{DM2} = 615~1341 Ma of the metallogenic granodiorite porphyry. The Hf isotope values $^{176}Hf/^{177}Hf$ = 0.2828596~0.2829451, and the ε_{Hf} (t) = +5.7~+8.8 of the diorite porphyrite, T_{DM2} = 827~1108 Ma, indicating that the ore-forming materials were the possible involvement of heterogeneous juvenile sources including moderately depleted mantle and newly underplated lower crust. The major and trace elements (including REEs) implied that these intrusions are the I-type granite and linked intimately to the westward subduction of the Paleo-Pacific Ocean plate. From these whole-rock major and trace elements and zircon U-Pb ages, as well as Sr-Nd-Hf isotope data, we conclude that the ore-associated I-type granites in the Bayanbaolege deposit formed in an extensional tectonic setting of the Early Cretaceous, and are compactly related to the retreat of the Paleo-Pacific Ocean subducted plate linked intimately to the westward subduction of the Paleo-Pacific Ocean plate rather than the closure of the Mongol–Okhotsk Ocean. Furthermore, by integrating geological background work and previous research work, implying the mineralization age of the Bayanbaolege deposit should have been formed in the 125–130 Ma.

Keywords: LA–ICP–MS U-Pb age; Hf isotope; petrogenesis; tectonic implication; Bayanbaolege deposit

Citation: Wang, X.; Yang, Q.; Sun, Z.-M.; Ren, Y.-S. Petrogenesis and Tectonic Implications of the Ore-Associated Intrusions in Bayanbaolege Ag Polymetallic Deposit, Inner Mongolia, NE China. *Minerals* **2022**, *12*, 912. https://doi.org/10.3390/min12070912

Academic Editor: Maria Boni

Received: 15 June 2022
Accepted: 18 July 2022
Published: 20 July 2022

1. Introduction

The Great Xing'an Range (GXR) polymetallic metallogenic belt is located in the eastern segment of the Central Asian Orogenic Belt (CAOB), northeast (NE) China (Figure 1a,b), which hosts numerous important metal deposits, such as porphyry Sn-Cu-Ag, Cu (Mo) and Cu, and skarn polymetallic and hydrothermal vein types (Figure 1c) [1]. These deposits mainly formed in the Late Jurassic and Early Cretaceous, with a minor amount in the Triassic-Permian [2]. The formation of these deposits in this area were closely related to the contemporary tectono-magmatic events, which are considered to be the results of the evolution of Paleo-Asian, Mongol–Okhotsk, and Paleo-Pacific tectonic regimes ([3] and references therein).

The east slope of the southern GXR hosts a series of large Cu polymetallic deposits, always considered a Cu polymetallic metallogenic belt. However, several large Ag-Pb-Zn deposits have been discovered in recent years (Figure 1c), showing a considerable Ag-Pb-Zn polymetallic mineralization potential in this area [2].

The large Bayanbaolege Ag polymetallic deposit occurs in the northeastern Tuquan-Linxi Fe (Sn)-Cu-Pb-Zn-Ag-Nb (Ta) metallogenic belt in the east slope of the southern GXR, which contains proven reserves including 1440.41 t Ag, 381,826.1 t Zn and 51,493.27 t Pb, with average grades of 187.8 g/t Ag, 2.75% Zn and 1.89% Pb. A series of studies about the Bayanbaolege deposit have been reported, mainly regarding deposit geology, ore-forming conditions, Rb-Sr isotopic dating, fluid evolution, and S-Pb stable isotopes of the sulfides (pyrite and sphalerite) [4,5]. Although Wang et al. [4] have reported that the granodiorite porphyry had relationships with the polymetallic mineralization spatially, temporally, and genetically. However, the sources of the material of the granodiorite porphyry and the post-ore diorite porphyrite, as well as the relationship between mineralization and magmatism, have not been well-constrained; especially how and to what extent the mixture of the crustal or mantle materials have been involved in the forming of the deposit are still not clear, which restricts the better understanding of the metallogenetic mechanism and regularity of the deposit.

In this study, the major trace elements (including REEs), and Sr-Nd-Hf isotopic data of the ore-associated intrusive rocks and the zircon U-Pb dating of the diorite porphyrite in the Bayanbaolege deposit are combined with the Sr-Nd isotopic data of the Early Cretaceous granitoids and the age of the diagenetic and metallogenic in the adjacent regions. In combination with previous results, we present these study data and aim to discuss the petrogenesis and tectonic setting of the ore-associated intrusions in the Bayanbaolege deposit, which have important implications for better understanding the geological evolution history and metallogenic process of this region.

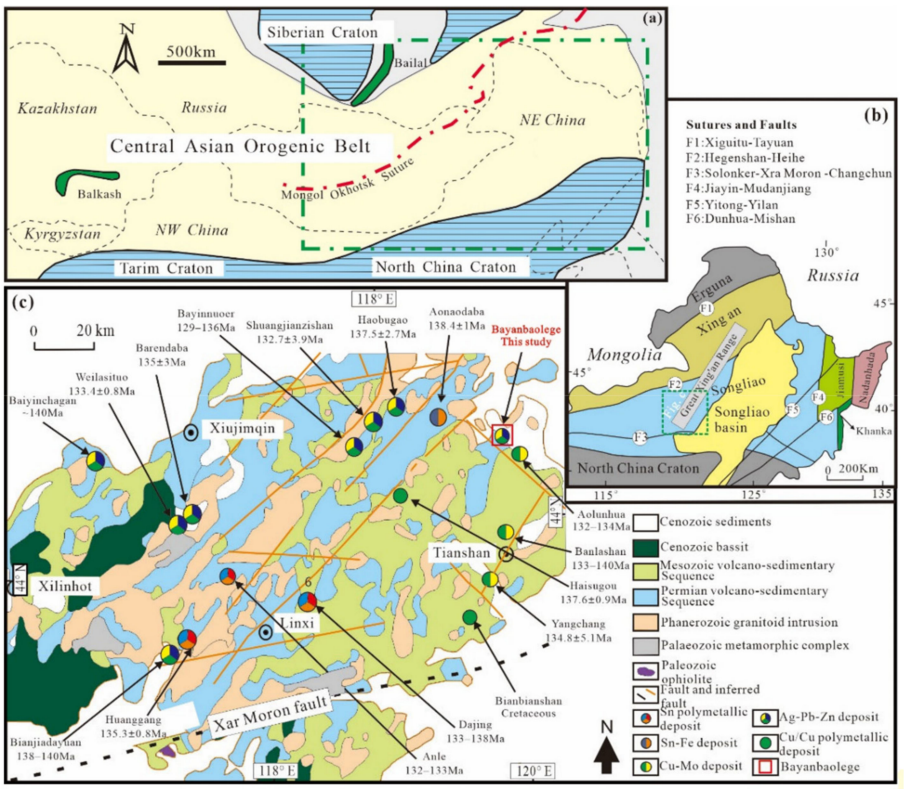

Figure 1. (**a**) Location of the Central Asian Orogenic Belt [1]; (**b**) simplified geotectonic division of northeastern China (modified after [6]); (**c**) regional geologic map of the southern Great Xing'an Range (modified after [1]).

2. Geological Setting

The large Bayanbaolege Ag polymetallic deposit is located in the Songliao block, which is considered to belong to the Xing'an-Mongolian Orogenic Belt (XMOB) in a tectonic unit of the eastern segment of the CAOB (Figure 1a,b). The XMOB is separated by the Xinlin–Xiguitu fault, Hegenshan–Heihe fault, and Solonker–Xar Moron–Changchun fault, dividing the XMOB into several elongated terranes including the Erguna, Xing'an, Songliao, and Jiamusi blocks (Figure 1b). The GXR is located in the eastern segment of the XMOB, NE China, which at least experienced the subduction closure of the Paleo-Asian Ocean, the closure of Mongol–Okhotsk Ocean, and the subduction of the Paleo-Pacific Ocean Plate, and resulted in widespread associated magmatism and metamorphism [7–9].

The regional strata are dominated by Permian and Mesozoic volcano-sedimentary rocks. The Permian strata include, from bottom to top, the Shoushangou Formation (P_1s), comprising thick-bedded limestone. The Dashizhai Formation (P_2d) is composed of slightly metamorphic intermediate-to-acidic lava, rhyolite, and volcaniclastics intercalated with some sandstone. The Zhesi Formation (P_2zs) consists of silty mudstone, tuffaceous sandstone, and tuffaceous silty sandstone intercalated with oolitic crystalline limestone lens. The Linxi Formation (P_3l) is composed of sandy conglomerate and siltstone intercalated. These formations are unconformably overlain by Mesozoic volcano-sedimentary sequences consisting of rhyolite, andesite, and felsic pyroclastic units. The Mesozoic strata, from oldest to youngest, consist of four formations, namely the Manketouebo, Manitu, Baiyingaolao, and Meiletu. The Manketouebo Formation is mainly composed of rhyoitic tuff with minor rhyolite and dacite. The Manitu Formation consists of andesite, trachy dacite, and volcaniclastic rocks. The Baiyingaolao Formation consists of rhyolite and rhyolitic tuff with intercalated sedimentary rocks. The Meiletu Formation is composed of basalt, basaltic andesite, andesite, and trachyte [10].

Faults and folds are well-developed in the GXR, which are widely distributed in this region. The faults are mainly NE- and NNE-trending and have overprinted existing EW-trending faults that dominate this area and control the Mesozoic-Paleozoic intrusive rocks. Regional magmatism includes Hercynian plutons (321–250 Ma), including quartz diorite, tonalite, granodiorite, monzogranite, gabbro, quartz monzonite, biotite granite, and K-feldspar granite [11–15]. Indosinian granitoids (250–225 Ma) consist of two-mica granite, granite porphyry [16,17], and granodiorite porphyry and Yanshanian intrusions (182–125 Ma) [1,4,9,16–18]. In addition, the W, Sn, Pb, Zn, Cu, and Ag deposits in the region are all closely related to Indosinian and Yanshanian granites, including granodiorite, quartz syenite, K-feldspar granite, hornblende monzonite, and monzogranite [2,6,14,16,19,20].

3. Deposit Geology

The Bayanbaolege deposit (44°36′ N, long. 119°57′ E) is located in Chifeng City, Inner Mongolia, NE China.

The strata in this ore district consist of the Zhesi Formation, the Linxi Formation, and the Manitu Formation (Figure 2). The Manitu Formation unconformably overlies the Zhesi Formation in the ore district and is composed of andesitic breccia clastic tuff, andesite, and dacite. The Linxi Formation consists of silty slate, sandy slate, and metamorphic fine sandstone. The Zhesi Formation consists of silty slate interbedded with a less argillaceous slate.

The NE–SW-trending F1 and F3 faults, and the NW–SE-trending F2 fault form a major tectonic framework in the ore district. The F1 and F3 faults control the distribution of intrusive and volcano-sedimentary rocks and are cut across by the F2 fault (Figure 2).

Two periods of magmatic activity have been identified in the ore district (Figures 2 and 3). The earlier period is represented by the granodiorite porphyry, which is spatial-temporal and genetically closely related to the polymetallic mineralization (Figure 4a,b) [4], and the latter is represented by diorite porphyrite (Figure 4c,d), which broke down the integrity of the ore body (Figure 4c).

The deposit consists of 86 sulfide–quartz vein-type polymetallic ore bodies, which show the characteristics of upper Ag bodies and lower Zn bodies as a whole, and distribute in the contact zone between the Late Permian strata and the Early Cretaceous granodiorite porphyry (Figure 3). The trend of these orebodies extends NE (16–67°) and dips along the NW with steep inclination (58–80°). Orebodies are 0.86–5.73 m thick, 38–1060 m in horizontal length, and 22–815 m in vertical depth. Ore structures consist of vein-type, and minor banded-type, brecciated-type and disseminated-type structures. The metallic minerals include pyrite, sphalerite, galena and minor chalcopyrite, cubanite, pyrrhotite, arsenopyrite, and loellingite. Gangue minerals include the quartz and calcite. The alterations developed such as limonitization, carbonatization, silicification and weak chloritization and epidotization.

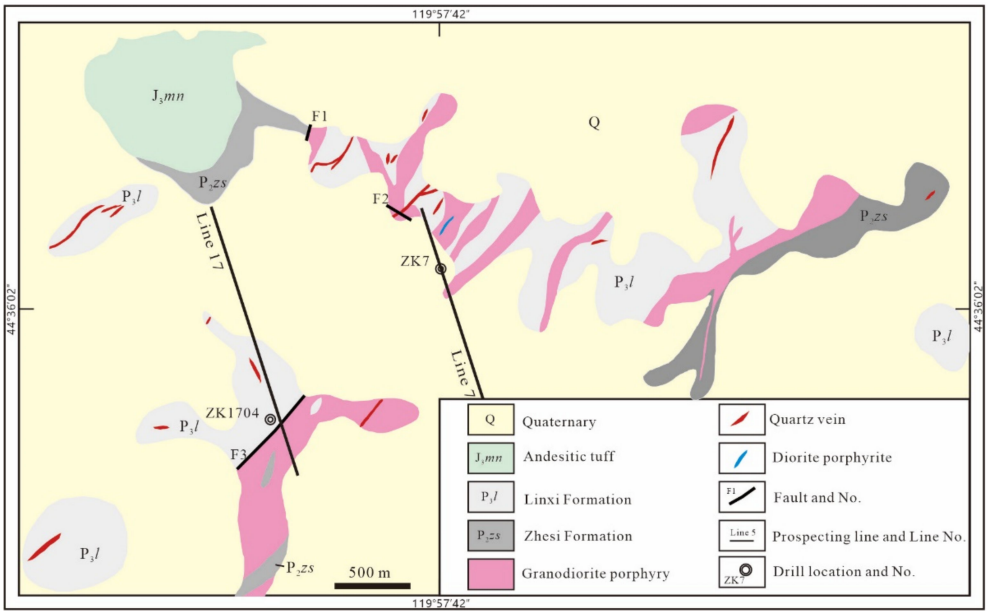

Figure 2. Geological sketch map, representative drill locations, and numbers in the Bayanbaolege deposit (modified after [4]).

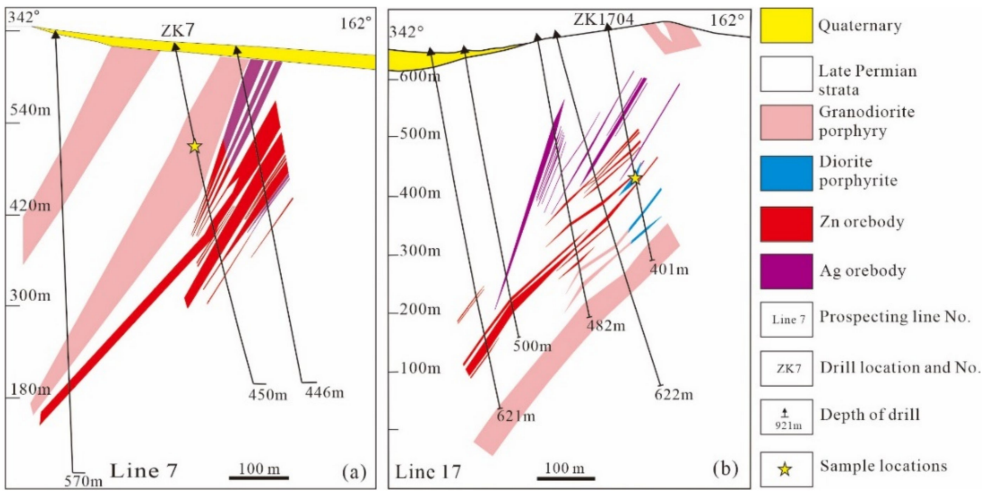

Figure 3. Geological section map of exploration lines and sampling locations in Bayanbaolege deposit (**a**,**b**).

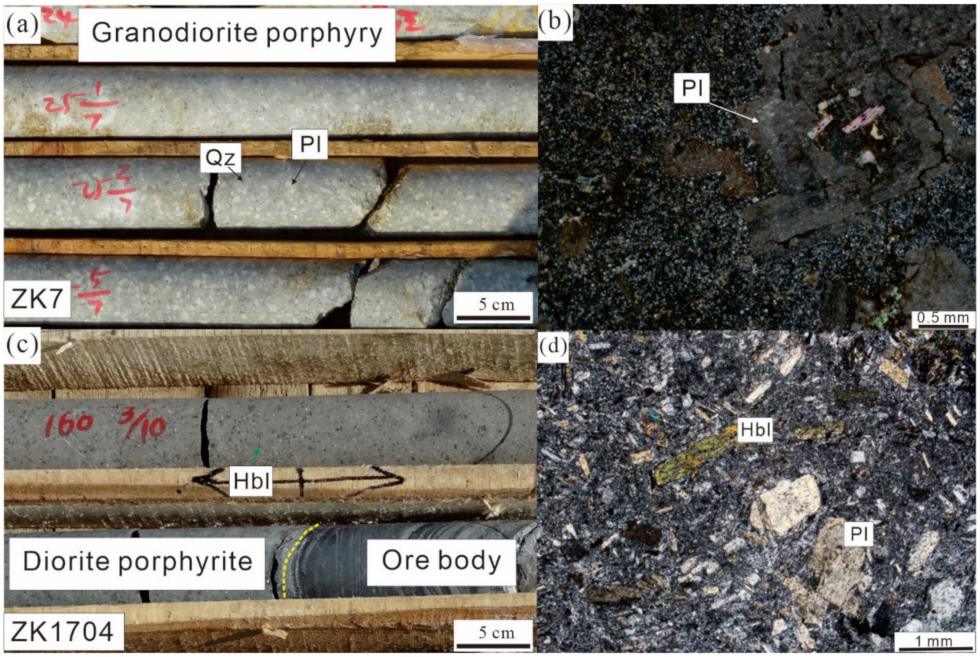

Figure 4. Representative field photographs and photomicrographs of the Bayanbaolege deposit. (**a**) Granodiorite porphyry consisting of plagioclase and minor quartz phenocrysts and matrixes. (**b**) Granodiorite porphyry showing the porphyritic texture with slight alteration of sericite. (**c**) Diorite porphyrite consisting of plagioclase and hornblende phenocrysts and microscopic matrix. (**d**) Porphyritic texture of the diorite porphyrite. Qz—quartz; Pl—plagioclase; Bt—biotite; Hbl—hornblende.

4. Sample Description and Analytical Methods

4.1. Sample Description

The granodiorite porphyry was selected (from drill hole ZK7) for Hf isotopic analyses, and five fresh samples (ZK7-1, ZK7-2, ZK7-3, ZK7-4, and ZK7-5) for whole-rock geochemistry and five samples (ZK7-T1, ZK7-T2, ZK7-T3, ZK7-T4 and ZK7-T5) of granodiorite porphyry for Sr-Nd isotopes (Figure 3a). The granodiorite porphyry is gray, with a massive structure (Figure 4a) and porphyritic texture (Figure 4b), contains phenocrysts and fine-grained groundmass with graphic texture. The principal minerals include alkali feldspar (~15%), plagioclase (~65%), quartz (~20%), biotite (~3%), and minor muscovite.

The diorite porphyrite was selected (ZK1704) for LA-ICP-MS zircon U-Pb dating and Hf isotopic analyses, and two samples (ZK1704-1 and ZK1704-2) without alterations for whole-rock geochemistry of diorite porphyrite, which obviously destroyed the integrity of the ore bodies, were selected from the ZK1704 drill core (Figure 3b). The diorite porphyrite has porphyritic texture and massive structure (Figure 4c,d), and the phenocryst minerals are dominated by plagioclase (15%–20%), alkali feldspar (5%–10%), and amphibole (<5%); the matrix minerals are composed of the plagioclase, alkali feldspar, quartz, amphibole, and biotite.

4.2. Analytical Methods

4.2.1. Ore-Forming Elements, Major and Trace Elements

Whole-rock major and trace elements of intrusive rock were analyzed at Tianjin Geological Mineral Testing Center, Tianjin, China. First, these samples were crushed in a steel jaw crusher and then powdered to 200 mesh in an agate mill, and then, trace element compositions were analyzed using the X-Series II ICP-MS (Thermo Electron Corporation, Waltham, MA, USA), following Qi et al. [21] and yielding an analytical precision better than 5%, and major element compositions were analyzed using X-ray fluorescence spectrometer (XRF), with a precision better than 2%. The selected samples were first characterized

in terms of chemical composition (major oxides wt.% and trace elements ppm) as listed in Table 1.

Table 1. Major, trace, and REE contents of intrusive rocks from Bayanbaolege deposit.

Sample	ZK7-1	ZK7-2	ZK7-3	ZK7-4	ZK7-5	ZK1704-1	ZK1704-2
Type	Granodiorite Porphyry					Diorite Porphyrite	
Major Elements (wt.%)							
Al_2O_3	12.91	12.79	13.76	12.87	12.71	16.24	16.41
CaO	1.21	1.26	1.25	1.23	1.22	3.41	2.43
TFeO	1.85	1.62	1.78	1.77	1.71	4.74	4.58
K_2O	5.26	4.04	4.73	4.85	5.16	4.3	4.35
MgO	0.43	0.32	0.41	0.32	0.31	2.71	1.86
MnO	0.07	0.06	0.07	0.08	0.07	0.43	0.38
Na_2O	3.8	4.89	4.13	3.98	4.55	3.6	3.24
P_2O_5	0.06	0.06	0.06	0.05	0.05	0.19	0.19
SiO_2	71.71	71.69	71.18	72.2	71.38	60.13	62.43
TiO_2	0.25	0.2	0.23	0.2	0.21	0.56	0.61
LOI	2.28	1.94	1.97	2	1.89	2.97	2.76
Total	99.83	98.87	99.57	99.55	99.26	99.28	99.22
$Na_2O + K_2O$	9.06	8.93	8.86	8.83	9.71	7.9	7.59
$(Na_2O + K_2O)/CaO$	7.49	7.09	7.09	7.18	7.96	2.32	3.13
A/NK	1.08	1.03	1.16	1.09	0.97	1.54	1.63
A/CNK	0.91	0.87	0.97	0.92	0.83	0.97	1.14
Trace elements (ppm)							
Li	13.3	15.04	12.87	12.92	14.37	47.45	35.62
Be	2.05	2.1	2.13	2.03	1.98	3.25	2.86
V	12.8	11.23	16.33	11.49	11.73	131.73	140.17
Cr	16.9	15.12	13.13	13.85	10.91	67.7	66.02
Co	2.04	1.7	2.04	1.77	1.78	8.94	22.5
Ni	2.45	1.71	2.15	2.33	2.2	22	40.77
Ga	22.82	24.07	22.76	22.09	23	23.21	24.52
Rb	116.08	133.02	151.5	185.42	119.19	137.42	160.68
Sr	36.13	145.21	22.79	51.74	132.49	44.36	49.64
Zr	156.26	185.26	161.99	200.44	229.71	241.09	226.94
Nb	8.75	9.25	8.26	8.51	9.17	13.78	13.49
Ba	915.22	927.81	855.86	815.69	884.61	405.26	580.88
La	29.68	38.97	26.8	30.19	31.08	37.04	35.53
Ce	57.85	72.44	52.53	57.8	59.83	77.75	73.75
Pr	6.72	8.44	6.2	6.74	7.04	9.43	9.24
Nd	24.22	30.14	22.79	24.42	25.39	37.24	35.65
Sm	4.36	5.15	4.23	4.35	4.64	7.52	6.81
Eu	0.79	0.86	0.78	0.75	0.79	1.66	1.84
Gd	3.74	4.38	3.56	3.73	3.93	6.24	5.96
Tb	0.6	0.68	0.58	0.6	0.66	1.02	0.96
Dy	3.39	3.72	3.35	3.3	3.67	5.78	5.61
Ho	0.68	0.74	0.66	0.66	0.73	1.15	1.1
Er	2.01	2.22	1.98	2.04	2.21	3.42	3.28
Tm	0.33	0.35	0.31	0.33	0.35	0.51	0.51
Yb	2.18	2.31	2.12	2.16	2.37	3.31	3.26
Lu	0.34	0.37	0.33	0.35	0.38	0.53	0.52
Y	18.85	20.79	19	19.06	20.92	29.93	28.49
Hf	5.05	5.64	4.93	5.85	6.64	7.15	6.67
Ta	0.85	0.89	0.81	1	0.9	0.95	0.93
Th	10.42	11.94	9.7	10.27	11.19	10.12	10.17
U	3.26	2.88	3.12	2.52	2.92	2.32	2.61
∑REE	136.89	170.76	126.23	137.42	143.07	192.62	184.02
LREE/HREE	9.32	10.56	8.79	9.44	9.01	7.77	7.68
10,000 Ga/Al	2.21	2.35	2.07	2.15	2.26	1.79	1.87

4.2.2. Sr-Nd Isotopes

Whole-rock Sr-Nd isotopes of the granodiorite porphyry were analyzed at the Isotopic Laboratory, Analytical Laboratory Beijing Research Institute of Uranium Geology, China National Nuclear Corporation, Beijing, China. Sr-Nd isotopic analyses were carried out at an ISOPROBE-T thermal ionization mass spectrometer (Thermo Fisher Scientific, Waltham, MA, USA), and with the $^{86}Sr/^{88}Sr$ ratio of 0.1194 and $^{146}Nd/^{144}Nd$ ratio

of 0.7219 for mass fractionation corrections. The analytical NBS987 Sr standard yields $^{87}Sr/^{86}Sr = 0.710250 \pm 0.000007$ (2σ) and the SHINESTU Nd standard yields $^{143}Nd/^{144}Nd = 0.512118 \pm 0.000003$(2σ).

4.2.3. Zircon U-Pb Dating and Hf Isotope

The zircon grain extraction and cathodoluminescence (CL) images were completed at the Institute of Regional Geology and Mineral Resources Survey, Langfang, Hebei Province, China. Zircons were extracted from the diorite porphyrite sample of No. ZK1704 and granodiorite porphyry sample of No. ZK7 using standard density and magnetic separation techniques, and cathodoluminescence (CL) images were obtained using a JSM-IT300 scanning electron microscope (JEOL, Tokyo, Japan). Zircon U-Pb isotopes were analyzed by a NEW WAVE 193 nm-FX ArF Excimer laser-ablation system (ESI Ltd., Beaverton, OR, USA) at the Isotopic Laboratory, Tianjin Institute of Geology and Mineral Resources of China Geological Survey, Tianjin, China. Samples analyses were carried out at an energy density of 11 J/cm^2, with a beam diameter of 30 μm and a repetition rate of 8 Hz. In situ zircon Hf isotopic analyses were measured on the same spot zones where U-Pb age determinations were previously analyzed, with a 50 μm laser beam diameter and a repetition rate of 11 Hz. Details of the operating conditions for the laser ablation system and the MC-ICP-MS instrument are described by Geng et al. [22]. The values of the isotopic ratios were calculated using ICPMS Data Cal 8.4 [23]. Concordia diagrams and weighted mean U-Pb ages were processed using ISOPLOT 3 [24]. Age data and Concordia plots were reported at one error and the uncertainties for weighted mean ages are given at a 95% confidence level.

5. Results

5.1. Major and Trace Elements

The granodiorite porphyry is characterized by high silica (SiO_2 = 71.18–72.20 wt.%), Al_2O_3 ranges from 12.71 to 13.76 wt.%, low MgO (0.31–0.43 wt.%) and is rich in alkali ($Na_2O + K_2O$ = 8.83–9.71 wt.%). K_2O/Na_2O ratios vary from 0.72 to 1.21, and the samples plotted in the high-k calc-alkaline field on the K_2O versus SiO_2 diagram. The molar ratio $Al_2O_3/(CaO + Na_2O + K_2O)$ (A/CNK) varies from 0.83 to 0.97, indicating the metaluminous character of all samples (Figure 5).

The diorite porphyrite samples are characterized by medium SiO_2 (SiO_2 = 60.13%–62.43%, mean = 61.28%), are rich in K_2O ($K_2O > Na_2O$), have medium CaO content (CaO = 2.43%–3.41%, mean = 2.92%), are rich in Al_2O_3 (Al_2O_3 = 16.24%–16.41%, mean = 16.33%) and have low MgO content (MgO = 1.86%–2.71%, mean = 2.29%), meaning that these samples are classified as transitional between metaluminous and peraluminous, and shoshonite series (Figure 5).

On the rare earth element (REE) chondrite-normalized spider diagram (Figure 6a), the granodiorite porphyry and diorite porphyrite rocks are characterized by the significant enrichment of light rare earth elements (LREEs) and by the variable depletion in heavy rare earth elements (HREEs). In the primitive mantle-normalized trace element spider diagrams (Figure 6b), all samples are relative enrichments in K, Rb, Th, and U, and depletions in Ba, Nb, Sr, P, and Ti.

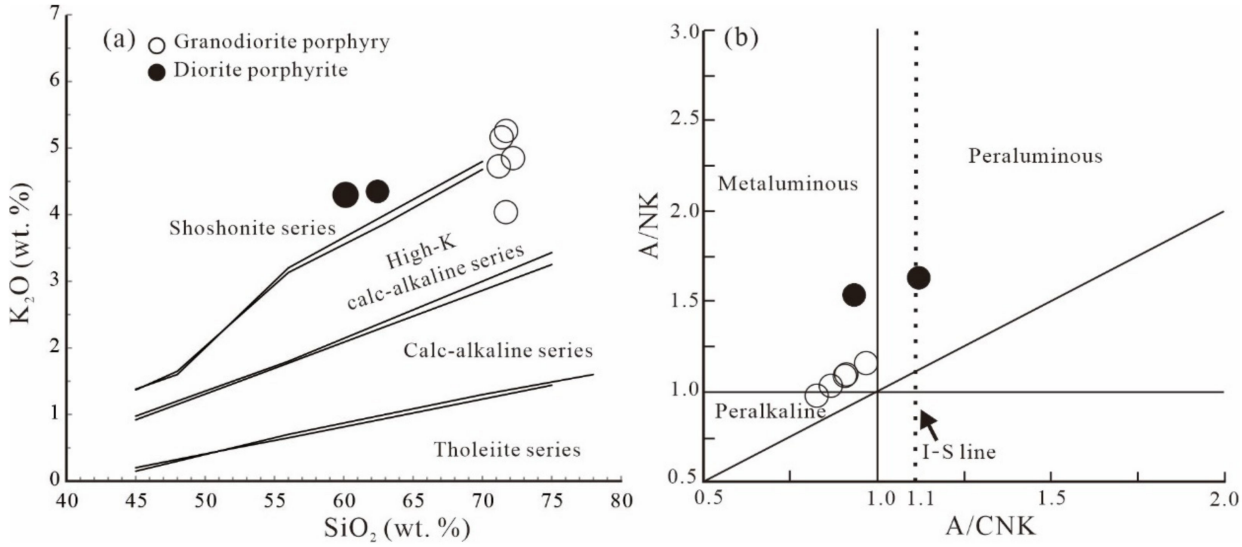

Figure 5. (**a**) K_2O versus SiO_2 [25] and (**b**) A/NK versus A/CNK diagrams [26] for the intrusions associated with the Bayanbaolege deposit.

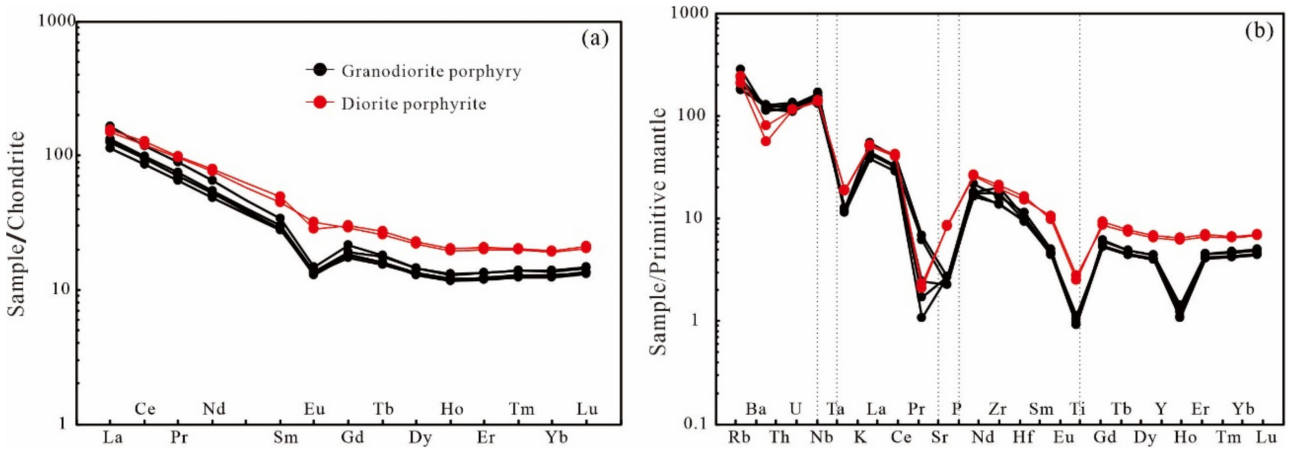

Figure 6. Chondrite-normalized REE (**a**) and primitive-mantle-normalized multi-element (**b**) diagrams for samples of the intrusions associated with the Bayanbaolege deposit (normalizing values are from [27]).

5.2. Sr-Nd Isotopes

Five samples of the granodiorite porphyry from the Bayanbaolege deposit were analyzed for Sr-Nd isotopic compositions, the aged-corrected (130 Ma) initial Sr and Nb isotope data for whole-rock samples, and the results are shown in Table 2. Initial ε_{Nd} (t) values of the samples range from −0.51 to 0.69 and $(^{87}Sr/^{86}Sr)_i$ isotope ratios vary from 0.708576 to 0.710536; all samples of the granodiorite porphyry have relatively homogeneous Nd-Sr isotopic compositions, which are consistent with the values of Mesozoic granites in NE China [28,29], and plotted within the overlapped field of the Mesozoic granites from NE China and the Mesozoic granitoids from CAOB in the ε_{Nd} (t) vs. $(^{87}Sr/^{86}Sr)_i$ diagram and the Phanerozoic granites of juvenile origin in NE China (Figure 7).

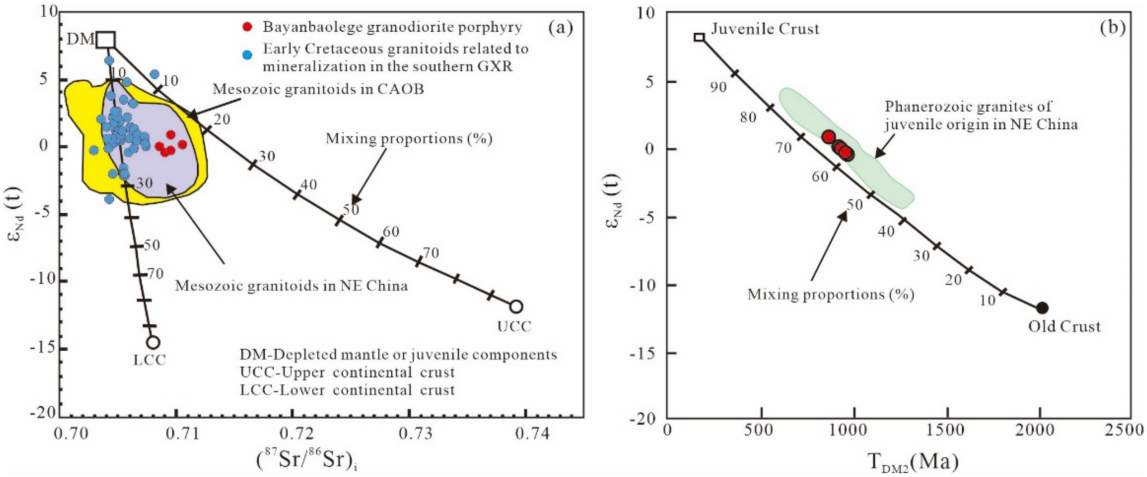

Figure 7. (**a**) ε_{Nd} (t) vs. $(^{87}Sr/^{86}Sr)_i$ isotopic ratio plot showing mixing proportions between two end members (modified after [29]). The area for Mesozoic granitoids in NE China is from [28,29]); Mesozoic granitoids in CAOB are from [30–32]; Early Cretaceous granitoids related to mineralization (data from Table 2); (**b**) ε_{Nd} (t) vs. T_{DM2} diagram [28], and the curve in this diagram approximates the proportions of mixing between juvenile and ancient crustal components. Data for Phanerozoic granites of juvenile origin in NE China are from [28].

5.3. Zircon U-Pb Dating and Lu-Hf Isotopes

Zircons grains collected from post-ore diorite porphyrite are euhedral-subhedral and obviously oscillatory growth-zoning in CL images (Figure 8a), and the value of the Th/U ratios range from 0.32 to 1.15. We interpret these zircons to be of igneous origin [32–34]. The LA-MC-ICP-MS zircon U-Pb dating results of post-ore diorite porphyrite are listed in Table 3. The analyses yielded $^{206}Pb/^{238}U$ ages ranging from 121 Ma to 129 Ma, with the weighted mean $^{206}Pb/^{238}U$ age of 124.8 ± 1.1 Ma (N = 18, MSWD = 2.6) (Figure 8b).

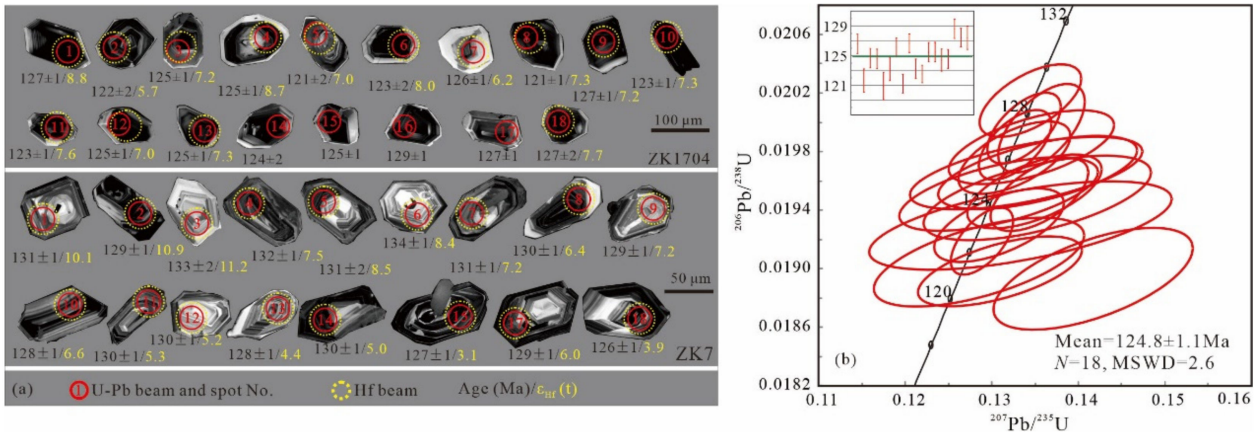

Figure 8. (**a**) Representative cathodoluminescence (CL) images of zircons from the granodiorite porphyry associated with mineralization (No. ZK7) and diorite porphyrite (No. ZK1704); (**b**) Zircon U-Pb Concordia diagrams of sample No. ZK1704.

Table 2. Early Cretaceous granitoids related to mineralization in southern Great Xing'an Range.

Deposits Name	Sample No.	Age (Ma)	Rb (ppm)	Sr (ppm)	$^{87}Rb/^{86}Sr$	$^{87}Sr/^{86}Sr$	2σ	$(^{87}Sr/^{86}Sr)_i$	Sm (ppm)	Nd (ppm)	$^{147}Sm/^{144}Nd$	$^{143}Nd/^{144}Nd$	2σ	T_{DM} (Ma)	T_{DM2} (Ma)	ε_{Nd} (t)	$f_{Sm/Nd}$	Reference
Bayanbaolege	zk7-T1	130	116.08	36.13	9.31	0.72672	18	0.70952	4.36	24.22	0.1088	0.512598	9	805	870	0.69	−0.45	This Paper
	zk7-T2	130	133.02	145.21	2.65	0.71544	14	0.71054	5.15	30.14	0.1032	0.512561	10	815	921	0.04	−0.48	
	zk7-T3	130	151.5	22.79	19.3	0.74471	17	0.70905	4.23	22.79	0.1123	0.51254	8	920	967	−0.5	−0.43	
	zk7-T4	130	185.42	51.74	10.39	0.72777	23	0.70858	4.35	24.42	0.1075	0.512556	4	855	935	−0.11	−0.45	
	zk7-T5	130	119.19	132.49	2.6	0.71432	22	0.70952	4.64	25.39	0.1104	0.512545	8	895	956	−0.38	−0.44	
Aolunhua	ALH-31	132	110.2	414.9	0.7686	0.70644	17	0.70498	3.21	19.67	0.0988	0.512631	5	689	801	1.5	−0.5	[9]
	ALH-32	132	99.81	533.4	0.5413	0.70602	18	0.70499	3.02	17.15	0.1066	0.512612	7	766	842	1	−0.46	
	ALH-44	132	70.26	383.4	0.5302	0.70619	11	0.70518	2.92	16.05	0.1099	0.512667	10	710	759	2.1	−0.44	
	ALH-54	132	102.7	448.2	0.6627	0.70609	11	0.70483	3.22	18.68	0.1043	0.512628	5	728	813	1.4	−0.47	
	ALH-56	132	65.3	203.4	0.9287	0.70665	25	0.70448	1.22	5.88	0.1251	0.512605	10	938	878	0.6	−0.36	
	ALH-63	132	79.12	519.2	0.4409	0.70596	14	0.70512	3.11	17.94	0.1047	0.512613	10	751	838	1.1	−0.47	
Haobugao	6-1	139	206	228	2.6193	0.71045	16	0.705268	7.39	33.1	0.135	0.512613	10		880	0.6		[35]
	6-2	139	191	224	2.4719	0.71009	14	0.705206	6.85	29.8	0.139	0.512627	14		862	0.82		
	6-3	139	279	74.1	10.9153	0.72764	18	0.706054	8.11	33.6	0.1459	0.512673	10		800	1.58		
	6-4	139	248	72.9	9.8622	0.7255	22	0.705996	8.04	32.4	0.15	0.512674	8		804	1.53		
	6-5	139	279	55.2	14.6526	0.73533	28	0.70636	7.29	26.7	0.165	0.512673	12		827	1.24		
Naoniushan	NNS-2-1	134			0.5855	0.70573	13	0.70458			0.1077	0.51268	9	678	737	2.4	−0.45	[36]
	NNS-2-2	134			0.4447	0.70557	13	0.70469			0.1116	0.512657	13	739	779	1.9	−0.43	
	JNNS-5a	134			0.2116	0.70538	14	0.70497			0.1155	0.512688	7	720	735	2.4	−0.41	
	JNNS-5b	134			0.2074	0.70535	13	0.70494			0.1113	0.512702	8	670	707	2.8	−0.43	
Baiyinnuoer	750-21-12	137	165	68.9	6.94	0.7193	12	0.70579	7.15	36.3	0.119	0.51269	7	743	737	2.4	−0.4	[37]
	BY13-6	137	207	142	4.24	0.71454	16	0.70632	7.36	38.2	0.1165	0.51274	9	646	654	3.4	−0.41	
	BY13-19	137	197	144	3.96	0.71363	14	0.70592	9.95	38.5	0.1562	0.512591	5	1485	948	−0.2	−0.21	
	BY13-20	137	181	124	4.23	0.71462	6	0.70639	7.29	37.1	0.1187	0.512645	6	813	808	1.5	−0.4	
	BY13-21	137	206	189	3.16	0.71087	9	0.70473	6.6	32.8	0.1215	0.512713	8	725	704	2.8	−0.38	
	BY13-49	137	193	142	3.92	0.71399	8	0.70632	8.12	41.6	0.1181	0.512608	9	867	866	0.8	−0.4	
	BY13-1	137	216	126	4.99	0.71724	9	0.70814	6.32	25.7	0.1487	0.51287	17	661	490	5.3	−0.24	
	750-21-6	129	229	40.8	16.2	0.73654	12	0.70668	5.02	26.2	0.1157	0.512622	8	824	841	1	−0.41	
	750-21-3	129	164	95.8	4.95	0.71485	14	0.70577	5.03	26	0.1172	0.521823	9	519	523	4.9	−0.4	
	750-25-9	129	199	41.9	13.8	0.7303	13	0.70505	5.3	28.7	0.1116	0.512632	6	776	819	1.3	−0.43	
	BY13-22	129	310	54	16.6	0.73527	11	0.70473	6.29	26.3	0.1446	0.512622	11	1168	879	0.5	−0.26	
	BY13-50	129	237	46.6	14.7	0.73155	12	0.70451	5.2	28.2	0.1114	0.512581	8	850	900	0.3	−0.43	
	BY13-51	129	333	66.4	14.5	0.73304	8	0.70637	4.7	25.1	0.1131	0.512567	9	886	925	0	−0.43	
Shuangjianzishan	SJS-3	137			0.3514	0.70509		0.70441			0.1134	0.512766		586	608	4	−0.42	[38]
	SJS-4	137			0.3058	0.70485		0.70425			0.111	0.512896		380	397	6.5	−0.44	

Table 2. *Cont.*

Deposits Name	Sample No.	Age (Ma)	Rb (ppm)	Sr (ppm)	$^{87}Rb/^{86}Sr$	$^{87}Sr/^{86}Sr$	2σ	$(^{87}Sr/^{86}Sr)_i$	Sm (ppm)	Nd (ppm)	$^{147}Sm/^{144}Nd$	$^{143}Nd/^{144}Nd$	2σ	T_{DM} (Ma)	T_{DM2} (Ma)	ε_{Nd} (t)	$f_{Sm/Nd}$	Reference
Haisugou	HSG01	137.6			1.01	0.70602	3	0.70403			0.1272	0.512657	5	869	799	1.6		[39]
	HSG02	137.6			0.996	0.70689	8	0.70494			0.1281	0.512633	2	921	838	1.1		
	HSG03	137.6			1.078	0.70706	4	0.70495			0.1199	0.512609	2	879	865	0.8		
	HSG09	137.6			0.939	0.70789	25	0.70605			0.1362	0.512623	2	1036	865	0.8		
	HSG41	137.6			1.106	0.70878	5	0.70661			0.132	0.512609	2	1009	882	0.6		
	HSG42	137.6			1.007	0.70728	12	0.70531			0.1264	0.512625	3	917	849	1		
	HSG43	137.6			1.029	0.70945	18	0.70743			0.1237	0.512583	2	960	911	0.2		
	HSG44	137.6			0.969	0.70723	3	0.70533			0.1354	0.512655	5	963	813	1.4		
	HSG45	137.6			1.3	0.70704	4	0.70449			0.1287	0.512619	2	952	861	0.8		
	HSG46	137.6			2.422	0.7121	16	0.70735			0.1268	0.512595	2	973	897	0.4		
	HSG47	137.6			1.083	0.70945	7	0.70733			0.1309	0.512593	11	1026	906	0.3		
	HSG48	137.6			1.624	0.70725	3	0.70406			0.1187	0.512607	3	872	866	0.8		
Baerzhe	Ba-6	125	10.1	1366	421	1.43636	7	0.68842	169.3	531.6	0.1279	0.51276	11		637	2.4	−0.35	[40]
	Ba-8	125	13.3	1364	296	1.22943	5	0.70356	172.4	510.2	0.2043	0.512761	18		724	2.24	0.04	
	Ba-14	125	9.05	1132	390	1.38568	4	0.69282	89	269.8	0.1813	0.512735	19		744	2.1	−0.08	
	Ba-16	125	10.15	920	274	1.18235	9	0.69557	64.3	214	0.1817	0.512754	10		714	2.47	−0.08	
	Ba-22	125	11.6	511	131	0.92987	6	0.69714	32.6	120.1	0.1641	0.512724	24		740	2.17	−0.17	
Yangchang	1-16	138			0.7992	0.70711		0.705546			0.0982	0.512459		914		−1.8	−0.5	[41]
	2-31	138			0.9214	0.70728		0.705479			0.1007	0.512476		911		−1.5	−0.49	
	2-32	138			0.956	0.70644		0.704573			0.1007	0.512461		931		−1.8	−0.49	
	3-3	138			0.7372	0.70691		0.705472			0.101	0.512453		944		−1.9	−0.49	
	3-4	138			0.9143	0.70733		0.705543			0.0964	0.512457		903		−1.8	−0.51	
	3-5	138			0.8772	0.70717		0.705459			0.0999	0.512457		931		−1.8	−0.49	
	4-23	138			0.7607	0.707		0.705512			0.0998	0.512447		942		−2	−0.49	
	5-8	138			0.9489	0.70738		0.705522			0.099	0.512454		927		−1.9	−0.5	
	6-7	138			0.6587	0.70692		0.705627			0.1021	0.512452		955		−2	−0.48	

Table 3. LA-MC-ICP-MS zircon U-Pb data of diorite porphyrite in the Bayanbaolege deposit.

Sample No.	Pb (ppm)	U (ppm)	Isotopic Ratios								Ages (Ma)					
			$^{232}Th/^{238}U$	1σ	$^{207}Pb/^{235}U$	1σ	$^{206}Pb/^{238}U$	1σ	$^{207}Pb/^{206}Pb$	1σ	$^{206}Pb/^{238}U$	1σ	$^{207}Pb/^{235}U$	1σ	$^{207}Pb/^{206}Pb$	1σ
ZK1704.1	7	338	0.7558	0.0020	0.1346	0.0078	0.0198	0.0002	0.0492	0.0028	127	1	128	7	158	135
ZK1704.2	17	810	0.9285	0.0141	0.1285	0.0099	0.0190	0.0002	0.0489	0.0034	122	2	123	9	145	163
ZK1704.3	18	874	0.6267	0.0026	0.1349	0.0063	0.0195	0.0002	0.0501	0.0024	125	1	129	6	200	113
ZK1704.4	6	306	0.9142	0.0044	0.1308	0.0094	0.0195	0.0002	0.0486	0.0034	125	1	125	9	130	165
ZK1704.5	3	159	0.4427	0.0029	0.1417	0.0094	0.0189	0.0003	0.0543	0.0035	121	2	135	9	383	147
ZK1704.6	4	197	0.6062	0.0011	0.1333	0.0143	0.0193	0.0002	0.0501	0.0054	123	2	127	14	200	250
ZK1704.7	10	500	0.6093	0.0022	0.1326	0.0053	0.0198	0.0002	0.0487	0.0019	126	1	126	5	132	90
ZK1704.8	9	422	1.0551	0.0031	0.1309	0.0077	0.0190	0.0002	0.0500	0.0029	121	1	125	7	196	136
ZK1704.9	24	1115	0.8224	0.0008	0.1327	0.0034	0.0198	0.0002	0.0485	0.0012	127	1	127	3	123	58
ZK1704.10	8	385	0.7000	0.0028	0.1308	0.0061	0.0193	0.0002	0.0492	0.0022	123	1	125	6	156	107
ZK1704.11	30	1309	1.1541	0.0058	0.1289	0.0029	0.0192	0.0002	0.0487	0.0011	123	1	123	3	134	51

Table 3. *Cont.*

Sample No.	Pb (ppm)	U (ppm)	Isotopic Ratios								Ages (Ma)					
			$^{232}Th/^{238}U$	1σ	$^{207}Pb/^{235}U$	1σ	$^{206}Pb/^{238}U$	1σ	$^{207}Pb/^{206}Pb$	1σ	$^{206}Pb/^{238}U$	1σ	$^{207}Pb/^{235}U$	1σ	$^{207}Pb/^{206}Pb$	1σ
ZK1704.12	9	429	0.7692	0.0007	0.1340	0.0110	0.0197	0.0002	0.0494	0.0040	125	1	128	10	169	189
ZK1704.13	7	318	0.6843	0.0019	0.1353	0.0094	0.0197	0.0002	0.0499	0.0034	125	1	129	9	191	160
ZK1704.14	5	261	0.4098	0.0054	0.1353	0.0107	0.0195	0.0002	0.0503	0.0040	124	2	129	10	211	184
ZK1704.15	30	1560	0.3169	0.0010	0.1355	0.0046	0.0195	0.0002	0.0504	0.0016	125	1	129	4	213	73
ZK1704.16	13	596	0.8334	0.0027	0.1345	0.0048	0.0201	0.0002	0.0484	0.0017	129	1	128	5	119	82
ZK1704.17	15	660	0.8707	0.0031	0.1337	0.0035	0.0200	0.0002	0.0486	0.0012	127	1	127	3	128	59
ZK1704.18	15	683	0.8212	0.0043	0.1357	0.0041	0.0200	0.0002	0.0493	0.0014	127	2	129	4	163	67

Table 4. Zircon Hf isotopic compositions of the granitoids from Bayanbaolege deposit.

No.	Age (Ma)	$^{176}Yb/^{177}Hf$	22σs	$^{176}Lu/^{177}Hf$	2σ	$^{176}Hf/^{177}Hf$	2σ	$^{176}Hf/^{177}Hf_i$	$e_{Hf}(0)$	$e_{Hf}(t)$	T_{DM}(Ma)	$T_{DM}{}^{C}$(Ma)	$f_{Lu/Hf}$
Granodiorite Porphyry													
ZK7.1	131	0.048202	0.000446	0.001713	0.000005	0.282979	0.000029	0.282975	7.3	10.1	394	714	−0.95
ZK7.2	129	0.113247	0.00233	0.003574	0.000038	0.283009	0.000043	0.283001	8.4	10.9	369	635	−0.89
ZK7.3	133	0.050256	0.000219	0.001714	0.000013	0.283009	0.000036	0.283005	8.4	11.2	350	615	−0.95
ZK7.4	132	0.036693	0.00089	0.001217	0.000021	0.282904	0.000033	0.282901	4.7	7.5	496	951	−0.96
ZK7.5	131	0.031451	0.000836	0.001101	0.000019	0.282932	0.000029	0.28293	5.7	8.5	455	860	−0.97
ZK7.6	134	0.069897	0.001611	0.002781	0.000049	0.282933	0.000031	0.282926	5.7	8.4	475	869	−0.92
ZK7.7	131	0.040393	0.000108	0.001661	0.000005	0.282898	0.000027	0.282894	4.5	7.2	511	975	−0.95
ZK7.8	130	0.036409	0.000931	0.001166	0.000019	0.282874	0.000028	0.282871	3.6	6.4	539	1049	−0.96
ZK7.9	129	0.051141	0.000582	0.001867	0.000016	0.2829	0.000027	0.282896	4.5	7.2	511	971	−0.94
ZK7.10	128	0.056866	0.001234	0.002098	0.000031	0.282884	0.000029	0.282879	4	6.6	538	1026	−0.94
ZK7.11	130	0.033501	0.000676	0.001388	0.000025	0.282844	0.000026	0.28284	2.5	5.3	585	1148	−0.96
ZK7.12	130	0.047709	0.000959	0.001722	0.000022	0.282843	0.000034	0.282838	2.5	5.2	592	1155	−0.95
ZK7.13	128	0.014286	0.000608	0.000547	0.000017	0.282817	0.000027	0.282816	1.6	4.4	609	1228	−0.98
ZK7.14	130	0.041769	0.001384	0.001424	0.000038	0.282836	0.000035	0.282832	2.3	5	597	1174	−0.96
ZK7.15	127	0.080624	0.002572	0.00278	0.000081	0.282788	0.000039	0.282781	0.6	3.1	691	1341	−0.92
ZK7.17	129	0.037943	0.000651	0.001404	0.000021	0.282866	0.000031	0.282863	3.3	6	554	1078	−0.96
ZK7.18	126	0.046771	0.000295	0.001917	0.000014	0.282808	0.000026	0.282804	1.3	3.9	645	1270	−0.94
Diorite porphyrite													
ZK1704.1	127	0.054425	0.000299	0.001397	0.000009	0.282945	0.000022	0.282942	6.1	8.8	440	827	−0.96
ZK1704.2	122	0.061272	0.000575	0.00146	0.000019	0.28286	0.00002	0.282856	3.1	5.7	564	1108	−0.96
ZK1704.3	125	0.043899	0.000121	0.001144	0.000002	0.282901	0.000018	0.282898	4.6	7.2	500	969	−0.97
ZK1704.4	125	0.023133	0.000345	0.000568	0.000006	0.282941	0.000018	0.28294	6	8.7	436	836	−0.98
ZK1704.5	121	0.028046	0.000244	0.000705	0.000004	0.282896	0.000023	0.282895	4.4	7	501	986	−0.98
ZK1704.6	123	0.053344	0.000572	0.001276	0.000009	0.282924	0.00002	0.282922	5.4	8	468	897	−0.96
ZK1704.7	126	0.031281	0.00036	0.00079	0.00001	0.282872	0.000017	0.28287	3.5	6.2	536	1058	−0.98
ZK1704.8	121	0.042613	0.000187	0.001056	0.000008	0.282905	0.000024	0.282903	4.7	7.3	493	961	−0.97
ZK1704.9	127	0.045652	0.000274	0.001133	0.000008	0.282899	0.000018	0.282896	4.5	7.2	503	974	−0.97
ZK1704.10	123	0.052782	0.000316	0.001312	0.000007	0.282904	0.000021	0.282901	4.7	7.3	497	962	−0.96
ZK1704.11	123	0.031526	0.000057	0.000801	0.000004	0.282911	0.000018	0.282909	4.9	7.6	481	936	−0.98
ZK1704.12	125	0.045432	0.000179	0.001123	0.000005	0.282895	0.00002	0.282892	4.3	7	509	989	−0.97
ZK1704.13	129	0.027104	0.000172	0.000639	0.000002	0.282901	0.000027	0.282899	4.6	7.3	494	961	−0.98
ZK1704.18	127	0.037908	0.000139	0.00091	0.000002	0.282914	0.000029	0.282912	5	7.7	478	922	−0.97

The crystallization age of the granodiorite porphyry associated genetically with the mineralization of the Bayanbaolege deposit is 130 ± 1 Ma [4]; the shapes of the zircon grain are shown in Figure 8a. In situ zircon Lu-Hf isotopic data of the granodiorite porphyry and the diorite porphyrite are shown in Table 4. The zircons of the No.ZK7 yielded initial $^{176}Hf/^{177}Hf$ ratios of 0.282788 to 0.283009 with ε_{Hf} (t) values of +3.1 to +11.2, and T_{DM2}(Hf) model ages of 615–1341 Ma. The zircons of the diorite porphyrite yielded initial $^{176}Hf/^{177}Hf$ ratios of 0.282856 to 0.282942 with ε_{Hf} (t) values of +5.7 to +8.8 and T_{DM2}(Hf) model ages of 827–1108 Ma. All analyses plot above the Chondrite uniform reservoir (CHUR) evolutionary line in a diagram of ε_{Hf} (t) vs. age (Figure 9a) and located in the region of Early Cretaceous magmatic rocks in the southern GXR (Figure 9b).

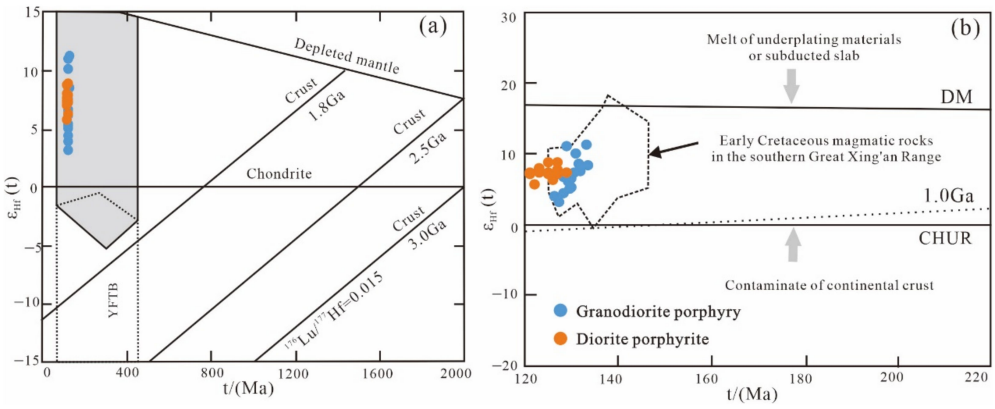

Figure 9. Correlations between ε_{Hf} (t) and ages of zircons from the intrusions. CAOB = Central Asian Orogenic Belt; YFTB = Yanshan Fold and Thrust Belt. (**a**) modified after [42,43]; (**b**) after [1,44].

6. Discussion

6.1. Petrogenesis of the Ore-Associated Intrusions

The major and trace elements of the intrusions are shown in Table 1. The granodiorite porphyry contains high concentrations of SiO_2, high K calc-alkalinity, metaluminous (A/CNK = 0.83–0.97), and sodium contents (3.80–4.89 wt.%); the CIPW normative corundum <1% and diopside of samples showed that the high-Si felsic granodiorite porphyry is I-type granites [45]. The high $(K_2O + Na_2O)/CaO$ (7.09–7.96), FeO^T/MgO ratios (4.30–5.53) and 10,000 Ga/Al ratios (2.07–2.35) are also showed in the I-type. The diorite porphyrite, A/CNK = 0.97–1.14, and A/NK = 1.54–1.63, metaluminous-peraluminous, and 10,000 Ga/Al = 1.79–1.87 samples all fall into the I-type granites field in Figure 10a,b [46].

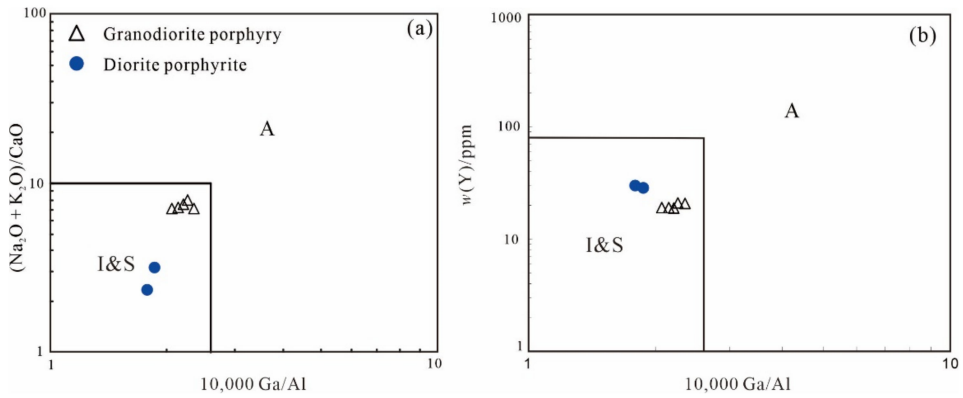

Figure 10. Discrimination diagrams of granite genetic type in the study area: (**a**) $(K_2O + Na_2O)/CaO$ vs. 10,000 Ga/Al; and (**b**) Y vs. 10,000 Ga/Al [46].

6.2. Magmatic Material Source of the Ore-Associated Intrusions

There are three possible interpretations for the source of I-type granites: (1) partial melting of metamorphic intermediate-basic igneous rocks from the crust [47,48]; (2) frac-

tional crystallization from mantle magma and assimilation of the crust material in the late stage of magma [49,50] and (3) magma mixing of basaltic magma with felsic magmas [51].

Table 1 showed that samples of granodiorite porphyry from the Bayanbaolege deposit contain low MgO (0.31–0.43 wt.%), Ni (1.71–2.45 ppm), and Cr (10.91–16.90 ppm) element, indicating a few involvements of mantle-derived magma [52,53]. The Nb/Ta ratios for the Bayanbaolege intrusion vary between 8.47 and 10.36, significantly lower than the mantle values (17.5 ± 2) [54,55] and close to the crust values (~11) [55,56]. Combined with the high SiO_2, K_2O, low Al_2O_3 and Sr, Nb, Ta, Ti and P, and Figure 6 showed the positive Rb, Th, and K anomalies, with enrichment in LREEs and LILEs. These geochemical features are commonly matched to crust-derived rocks [57]. Hence, the granodiorite porphyry from the Bayanbaolege deposit is likely to have come from a crustal source or a mixing of the mantle- and crustal-derived magmas. The granodiorite porphyry yielded the ε_{Nd} (t) values ranging from −0.51 to 0.69 and a young two-stage Nd model age (T_{DM2} =870–967 Ma), indicating that the primary magmas were extracted from a mixed juvenile-crust and old-crust source (Figure 7).

The diorite porphyrite exhibited low SiO_2 (60.13–62.43 wt.%), high K_2O (4.30–4.35 wt.%), and Al_2O_3 (16.24–16.41 wt.%) contents, suggesting that these rocks are metaluminous-peraluminous. The trace elements diagrams in Figure 6 show that the diorite porphyrite and the granodiorite porphyry have a similar tendency. The Nb/Ta values (14.48–14.56) are higher than the crust values (11.0) and lower than those of the primitive mantle (17.5 ± 2) [55], implying these rocks are from the mixing of the mantle- and crustal-derived magmas.

These rocks of the diorite porphyrite and granodiorite porphyry have positive ε_{Hf} (t) (+5.7 to +8.8) and (+3.1 to +11.2), and T_{2DM} ages (827~1108 Ma) and (615~1341 Ma), respectively (Table 4). All analyses plot above the Chondrite uniform reservoir (CHUR) evolutionary line in a diagram of ε_{Hf} (t) vs. age (Figure 9a) located in the region of Early Cretaceous magmatic rocks in the southern GXR (Figure 9b). The similar εHf(t) values of these samples and the wider ranges and more mantle-like values suggest the possible involvement of heterogeneous juvenile sources, including moderately depleted mantle and newly underplated lower crust.

6.3. Mineralization Age of Polymetallic Mineralization

There are two main methods for determining the mineralization age of hydrothermal deposits. One is indirect, using the isotopic ages of rocks (strata or intrusions) associated with mineralization; the other directly measures the ages of ore minerals or coexistence alteration minerals with ore minerals [58]. The indirect mineralization age of the granodiorite porphyry associated genetically with mineralization reported is 130 ± 1 Ma [4] and the direct isochron age of sphalerite is 129.9 ± 2.9 Ma [5]. Hence, the mineralization of the Bayanbaolege deposit occurred in the Early Cretaceous. However, the Bayanbaolege is a large-scale polymetallic deposit including Ag, Zn, and Pb. The different metallogenic temperatures and precipitation phases of these metals have been verified by Wang et al. [4]. The mineralization of these metals should last quite a long time. However, the indirect mineralization age (130 ± 1 Ma) and the direct mineralization age (129.9 ± 2.9 Ma) are too close. To constrain the mineralization duration of the Bayanbaolege polymetallic deposit, the diorite porphyrite was measured and weighted with a mean $^{206}Pb/^{238}U$ age of 124.8 ± 1.1 Ma (Figure 8b). These results of the magmatism and mineralization mentioned above give a range of 125–130 Ma, and this result is consistent with the mineralization age (126–132 Ma) of the nearby Aolunhua porphyry Mo-Cu deposit [59]. Meanwhile, the mineralization age of the lager-scale Baiyinnuoer skarn Pb-Zn deposit (129–136 Ma) [37] and the lager-scale Dajing Sn-Cu-Pb-Zn-Ag (133–136 Ma) [60] also show that the hydrothermal mineralization is probably the product of the large-scale tectono-magmatic-mineralization events in the southern GXR in the Early Cretaceous.

6.4. Tectonic Implications

The tectonic setting of the Late Mesozoic magmatism in the southern GXR and adjacent areas has been controversial and invoked (1) post-orogenic extension after the closure of the Mongol–Okhotsk Ocean [32,61–66] and (2) the subduction of the Paleo–Pacific Ocean Plate [67–72]. Recent studies considered that the GXR was subject to an extensional tectonic regime related to the delamination of a thickened crust [73–76], which was identified by the large-area distributed synchronous A-type granitoids [77], metamorphic core complexes [78–80], diabase dyke groups, and rift basins [81,82]. Hence, the GXR was in an extensional setting during the Early Cretaceous, which resulted from post-orogenic extensional tectonics after the closure of the Mongol–Okhotsk Ocean, or the subduction of the Paleo-Pacific Ocean Plate.

The extensional environment during the 138–145 Ma was the common result of the closure of the Mongolia–Okhotsk Ocean and the subduction of the Paleo-Pacific Ocean Plate [83–85], and the active continental margin setting of the 106–133 Ma mainly related to the subduction of the Paleo-Pacific Ocean Plate [83,86]. Furthermore, there is a large crossing angle between the tendency (NE) of the Mongol–Okhotsk Ocean suture zone and the tendency (NNE) of the GXR, implying that the Mongol–Okhotsk Ocean tectonic domain cannot efficaciously control the Early Cretaceous magmatism in the GXR area [87,88].

The diorite porphyrite and granodiorite porphyry magmatism of the Bayanbaolege took place in the Early Cretaceous (125 Ma and 130 Ma), and seven samples plotted in the VAG field (Figure 11a–c) and the subduction zone field (Figure 11d) in the geochemical discrimination diagrams, indicating that the granitoids in the Bayanbaolege area have closely related to the subduction tectonic setting instead of the post Mongol–Okhotsk Ocean tectonic regime. This result is consistent with the point that the influence scope of the Paleo-Pacific plate subduction extended to the GXR during the period of the Early Cretaceous [89]. So, it can be concluded that the affected region of the westward subduction of the Paleo-Pacific Ocean plate reached the east slope of the Great Xing'an Range during the early Cretaceous. This viewpoint is also consistent with the thoughts of Zhu [90] and Tian et al. [91], who thought that the gravity gradient zones began to form in the early cretaceous and did not cross the GXR, in other words, the leading edge of the subduction Paleo-Pacific Ocean plate stagnates in the east segment of the GXR.

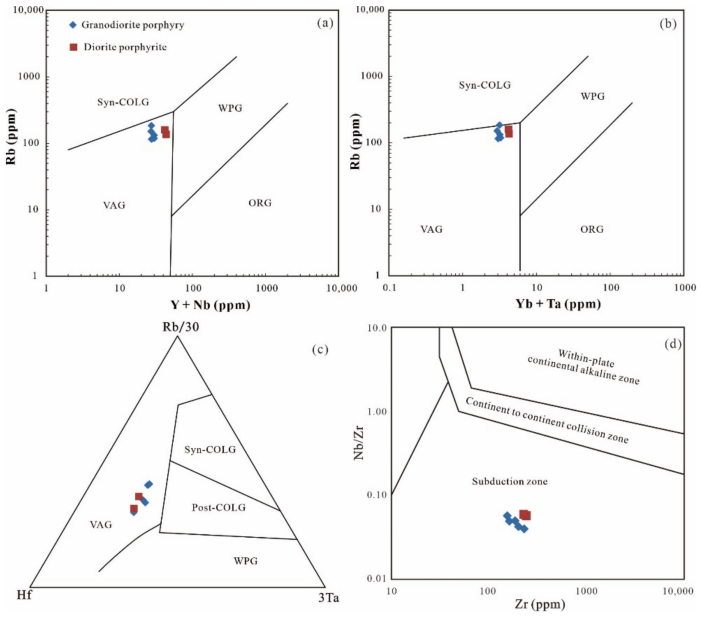

Figure 11. (**a**) Y vs. Nb diagram [92]; (**b**)Y + Nb vs. Rb diagram [92]; (**c**) Rb/30–Hf–3Ta discrimination diagram [93]; (**d**) Zr versus (Nb/Zr) diagram [94]. Abbreviations: VAG—volcanic arc granite; ORG—ocean ridge granite; WPG—within-plate granite; Syn-COLG—syncollision granite.

7. Conclusions

The magmatism in the Bayanbaolege area occurred during the Early Cretaceous (diorite porphyrite: 124.8 ± 1.1 Ma), and the mineralization age should be formed in the 125–130 Ma. The whole-rock elemental compositions of the intrusions implied that the intrusive rocks are the I-type granite. The Sr-Nd-Hf isotopes indicated that the primary magmas of the granodiorite porphyry and the diorite porphyrite were the possible involvement of heterogeneous juvenile sources including moderately depleted mantle and newly underplated lower crust. The Early Cretaceous intrusive rocks in the Bayanbaolege area were formed in an extensional tectonic setting and compactly related to the retreat of the Paleo-Pacific Ocean subducted plate rather than the closure of the Mongol–Okhotsk Ocean.

Author Contributions: Conceptualization, X.W., Q.Y. and Y.-S.R.; field investigation, X.W., Q.Y. and Y.-S.R.; experimental analysis, X.W.; software, X.W. and Q.Y.; validation, X.W., Q.Y. and Y.-S.R.; resources, Y.-S.R. and Z.-M.S.; data curation, X.W.; writing—original draft preparation, X.W.; writing—review and editing, X.W. and Y.-S.R.; visualization, X.W.; funding acquisition, X.W. and Y.-S.R. All authors have read and agreed to the published version of the manuscript.

Funding: This work was financially supported by the Self-determined Foundation of Key Laboratory of Mineral Resources Evaluation in Northeast Asia, Ministry of Natural Resources (No. DBY-ZZ-19-10) and the China Geological Survey Programs (No. DD20160048; No. 12120115031701).

Acknowledgments: We sincerely appreciate the geologists from the Inner Mongolia Chifeng Geology and Mineral Resources Exploration Development Institute for their support of our fieldwork.

Conflicts of Interest: The authors declare no conflict of interest.

References

1. Ouyang, H.G.; Mao, J.W.; Zhou, Z.H.; Su, H.M. Late Mesozoic metallogeny and intracontinental magmatism, southern Great Xing'an Range, northeastern China. *Gondwana Res.* **2015**, *27*, 1153–1172. [CrossRef]
2. Zeng, Q.D.; Liu, J.M.; Chu, S.X.; Guo, Y.P.; Gao, S.; Guo, L.X.; Zhai, Y.Y. Poly-metal mineralization and exploration potential in southern segment of the Great Xing'an range. *J. Jilin Univ.* **2016**, *46*, 1100–1123. (In Chinese with English abstract)
3. Gao, Y.; Liu, J.; Li, T.G.; Zhang, D.D.; Yang, Y.C.; Han, S.J.; Ding, Q.F.; Zhang, S. Multiple isotope (He-Ar-Zn-Sr-Nd-Pb) constraints on the genesis of the Jiawula Pb-Zn-Ag deposit, NE China. *Ore Geol. Rev.* **2021**, *134*, 104142. [CrossRef]
4. Wang, X.; Ren, Y.S.; Zhao, D.S.; Ren, X.G. Ore-forming fluids and ore genesis of the large Bayanbaolege Ag polymetallic deposit, Southern Great Xing'an Range, NE China. *Ore Geol. Rev.* **2019**, *111*, 102987. [CrossRef]
5. Wang, X.; Ren, Y.S.; Yang, Q.; Zhao, D.S. Rb–Sr dating of sulfdes and S–Pb isotopic study of the Bayanbaolege Ag polymetallic deposit, Inner Mongolia, NE China. *Geochemistry* **2021**, *81*, 125724. [CrossRef]
6. Zhang, J.H.; Gao, S.; Ge, W.C.; Wu, F.Y.; Yang, J.H.; Wilde, S.A.; Li, M. Geochronology of the Mesozoic volcanic rocks in the Great Xing'an Range, northeastern China: Implications for subduction-induced delamination. *Chem. Geol.* **2010**, *276*, 144–165. [CrossRef]
7. Jahn, B.-M.; Wu, F.Y.; Chen, B. Massive granitoid generation in central Asia: Nd isotopic evidence and implication for continental growth in the Phanerozoic. *Episodes* **2000**, *23*, 82–92. [CrossRef]
8. Wu, F.Y.; Zhao, G.C.; Sun, D.Y.; Wilde, S.A.; Zhang, G.L. The Hulan Group: Its role in the evolution of the Central Asian Orogenic Belt of NE China. *J. Asian Earth Sci.* **2007**, *30*, 542–556. [CrossRef]
9. Liu, Y.J.; Li, W.M.; Feng, Z.Q.; Wen, Q.B.; Neubauer, F.; Liang, C.Y. A review of the Paleozoic tectonics in the eastern part of Central Asian Orogenic Belt. *Gondwana Res.* **2017**, *43*, 123–148. [CrossRef]
10. Bureau of Geology and Mineral Resources of Inner Mongolia (BGMRIM). *Regional Geology of Nei Mongol (Inner Mongolia) Autonomous Region*; Geological Publishing House: Beijing, China, 1991; 725p. (In Chinese with English abstract)
11. Li, J.Y. Permian geodynamic setting of Northeast China and adjacent regions: Closure of the Paleo–Asian Ocean and subduction of the Paleo-Pacific Plate. *J. Asian Earth Sci.* **2006**, *26*, 207–224. [CrossRef]
12. Bao, Q.Z.; Zhang, C.J.; Wu, Z.L.; Wang, H.; Li, W.; Sang, J.H.; Liu, Y.S. SHRIMP U-Pb zircon geochronology of a Carboniferous quartz-diorite in Baiyingaole area, Inner Mongolia and its implications. *J. Jilin Univ.* **2007**, *37*, 15–23. (In Chinese with English abstract)
13. Zhang, J.H.; Ge, W.C.; Wu, F.Y.; Wilde, S.A.; Yang, J.H.; Liu, X.M. Large-scale Early Cretaceous volcanic events in the northern Great Xing'an Range, Northeastern China. *Lithos* **2008**, *102*, 138–157. [CrossRef]
14. Wu, F.Y.; Sun, D.Y.; Ge, W.C.; Zhang, Y.B.; Grant, M.L.; Wilde, S.A.; Jahn, B.M. Geochronology of the Phanerozoic granitoids in northeastern China. *J. Asian Earth Sci.* **2011**, *41*, 1–30. [CrossRef]

15. Xue, H.M.; Guo, L.J.; Hou, Z.Q.; Tong, Y.; Pan, X.F.; Zhou, X.W. SHRIMP zircon U-Pb ages of the middle Neopaleozoic unmetamorphosed magmatic rocks in the southwestern slope of the Da Hinggan Mountain, Inner Mongolia. *Acta Petrol. Miner.* **2010**, *29*, 811–823. (In Chinese with English abstract)
16. Ge, W.C.; Wu, F.Y.; Zhou, C.Y.; Zhang, J.H. Zircon U-Pb ages and its significance of the Mesozoic granites in the Wulanhaote region, central Da Hinggan Mountain. *Acta Petrol. Sin.* **2005**, *21*, 749–762. (In Chinese with English abstract)
17. Jiang, S.H.; Nie, F.J.; Bai, D.M.; Liu, Y.F.; Liu, Y. Geochronology evidence for Indosinian mineralization in Baiyinnuoer Pb-Zn deposit of Inner Mongolia. *Miner. Depos.* **2011**, *30*. 787–798. (In Chinese with English abstract)
18. Gu, Y.C.; Chen, R.Y.; Jia, B.; Ju, N. Zircon U-Pb Dating and Geochemistry of the Granite Porphyry from the Shuangjianzishan Silver Polymetallic Deposit in Inner Mongolia and Tectonic Implications. *Geol. Prospect.* **2017**, *53*, 495–507. (In Chinese with English abstract)
19. Zeng, Q.D.; Qin, K.Z.; Liu, J.M.; Li, G.M.; Zhai, M.G.; Chu, S.X.; Guo, Y.P. Porphyry molybdenum deposits in the Tianshan-Xingmeng orogenic belt, northern China. *Int. J. Earth Sci.* **2015**, *104*, 991–1023. [CrossRef]
20. Li, M.W. Research on Metallogenic Series and Prognosis of End Ogenetic Metallic Deposits in the Middle Section of Tianshan-Xingmeng Orogeny. Ph.D. Thesis, Chinese Academy of Geological Sciences, Beijing, China, 2006; pp. 1–172. (In Chinese with English abstract)
21. Qi, L.; Hu, J.; Gregoire, D.C. Determination of trace elements in granites by inductively coupled plasma-mass spectrometry. *Talanta* **2000**, *51*, 507–513.
22. Geng, J.Z.; Qiu, K.F.; Gou, Z.Y.; Yu, H.C. Tectonic regime switchover of Triassic Western Qinling Orogen: Constraints from LA-ICP-MS zircon U-Pb geochronology and Lu-Hf isotope of Dangchuan intrusive complex in Gansu, China. *Chem. Erde Geochem.* **2017**, *77*, 637–651. [CrossRef]
23. Liu, Y.S.; Gao, S.; Hu, Z.C.; Gao, C.G.; Zong, K.Q.; Wang, D.B. Continental and oceanic crust recycling-induced melt-peridotite interactions in the Trans-North China Orogen: U-Pb dating, Hf isotopes and trace elements in zircon s of mantle xenoliths. *J. Petrol.* **2010**, *51*, 537–571. [CrossRef]
24. Ludwig, K.R. *Isoplot v. 3.0: A Geochronological Toolkit for Microsoft Excel*; Berkeley Geochronology Center: Berkeley, CA, USA, 2003; pp. 1–70.
25. Peccerillo, A.; Taylor, S.R. Geochemistry of Eocene calc-alkaline volcanic rocks from the Kastamonu area, northern Turkey. *Contrib. Mineral. Petrol.* **1976**, *58*, 63–81. [CrossRef]
26. Maniar, P.D.; Piccoli, P.M. Tectonic discrimination of granitoids. *Geol. Soc. Am. Bull.* **1989**, *101*, 635–643. [CrossRef]
27. Sun, S.S.; McDonough, W.F. *Chemical and Isotopic Systematics of Oceanic Basalts: Implications for Mantle Composition and Processes*; Geological Society: London, UK, 1989; Volume 42, pp. 313–345.
28. Wu, F.Y.; Jahn, B.M.; Wilde, S.; Sun, D.Y. Phanerozoic crustal growth: U-Pb and Sr–Nd isotopic evidence from the granites in northeastern China. *Tectonophysics* **2000**, *328*, 89–113. [CrossRef]
29. Wu, F.Y.; Jahn, B.M.; Wilde, S.A.; Lo, C.H.; Yui, T.F.; Lin, Q.; Ge, W.C.; Sun, D.Y. Highly fractionated I-type granites in NE China (II): Isotopic geochemistry and implications for crustal growth in the Phanerozoic. *Lithos* **2003**, *67*, 191–204. [CrossRef]
30. Jian, P.; Liu, D.; Kröner, A.; Windley, B.F.; Shi, Y.; Zhang, F.; Shi, G.; Miao, L.; Zhang, W.; Zhang, Q.; et al. Time scale of an early to mid-Paleozoic orogenic cycle of the long-lived Central Asian Orogenic Belt, Inner Mongolia of China: Implications for continental growth. *Lithos* **2008**, *101*, 233–259. [CrossRef]
31. Chen, B.; Jahn, B.M.; Tian, W. Evolution of the Solonker suture zone: Constraints from zircon U-Pb ages, Hf isotopic ratios and whole-rock Nd-Sr isotope compositions of subduction and collision-related magmas and forearc sediments. *J. Asian Earth Sci.* **2009**, *34*, 245–257. [CrossRef]
32. Jahn, B.M.; Litvinovsky, B.A.; Zanvilevich, A.N.; Reichow, M. Peralkaline granitoid magmatism in the Mongolian-Transbaikalian Belt: Evolution, petrogenesis and tectonic significance. *Lithos* **2009**, *113*, 521–539. [CrossRef]
33. Pupin, J.P. Zircon and granite petrology. *Contrib. Mineral. Petrol.* **1980**, *73*, 207–220. [CrossRef]
34. Koschek, G. Origin and significance of the SEM cathodoluminescence from zircon. *J. Microsc.* **1993**, *171*, 223–232. [CrossRef]
35. Wang, X.D.; Xu, D.M.; Lv, X.B.; Wei, W.; Mei, W.; Fan, X.J.; Sun, B.K. Origin of the Haobugao skarn Fe-Zn polymetallic deposit, Southern Great xing'an range, NE China: Geochronological, geochemical, and Sr-Nd-Pb isotopic constraints. *Ore Geol. Rev.* **2018**, *94*, 58–72. [CrossRef]
36. Gu, J.F.; Ni, P.; Li, W.S.; Wang, G.G.; Pan, J.Y.; Liu, Z. The characteristics of ore-forming fluid and genesis of the Matou Mo deposit, Chizhou, Anhui province. *J. Nanjing Univ.* **2018**, *54*, 351–365. (In Chinese with English abstract)
37. Jiang, S.H.; Chen, C.L.; Bagas, L.; Liu, Y.; Han, N.; Kang, H.; Wang, Z.H. Two mineralization events in the Baiyinnuoer Zn-Pb deposit in InnerMongolia, China: Evidence from field observations, S-Pb isotopic compositions and U-Pb zircon ages. *J. Asian Earth Sci.* **2017**, *144*, 339–367. [CrossRef]
38. Wang, F.X. Magmatism and Ag-Polymetallic Mineralization in Shuangjianzishan Deposit and Its Periphery, Inner Mongolia. Ph.D. Thesis, Chinese Academy of Geological Sciences, Wuhan, China, 2017; pp. 1–189. (In Chinese with English abstract)
39. Shu, Q.H.; Lai, Y.; Wang, C.; Xu, J.J.; Sun, Y. Geochronology, geochemistry and Sr-Nd-Hf isotopes of the Haisugou porphyry Mo deposit, northeast China, and their geological significance. *J. Asian Earth Sci.* **2014**, *79*, 777–791. [CrossRef]
40. Wang, Y.X.; Zhao, Z.H. Geochemistry and origin of the Baerzhe REE-Nb-Be-Zr super-large deposit. *Geochimica* **1997**, *26*, 24–35. (In Chinese with English abstract)

41. Zeng, Q.D.; Yang, J.H.; Zhang, Z.L.; Liu, J.M.; Duan, X.X. Petrogenesis of the Yangchang Mo-bearing granite in the Xilamulun metallogenic belt: China Office of Nuclear Energy, geochemistry, zircon U–Pb ages, and Sr–Nd–Pb isotopes. *Geol. J.* **2014**, *49*, 1–14. [CrossRef]
42. Yang, J.H.; Wu, F.Y.; Wilde, S.A.; Xie, L.W.; Yang, Y.H.; Liu, X.M. Tracing magma mixing in granite genesis: In situ U–Pb dating and Hf-isotope analysis of zircons. *Contrib. Mineral. Petrol.* **2007**, *153*, 177–190. [CrossRef]
43. Tang, J.; Xu, W.L.; Wang, F.; Zhao, S.; Wang, W. Early Mesozoic southward subduction history of the Mongol-Okhotsk oceanic plate: Evidence from geochronology and geochemistry of Early Mesozoic intrusive rocks in the Erguna Massif, NE China. *Gondwana Res.* **2016**, *31*, 218–240. [CrossRef]
44. Yao, L.; Lv, Z.C.; Ye, T.Z.; Pang, Z.S.; Jia, H.X.; Zhang, Z.H.; Wu, Y.F.; Li, R.H. Zircon U-Pb age, geochemical and Nd-Hf isotopic characteristics of quartz porphyry in the Baiyinchagan Sn polymetallic deposit, Inner Mongolia,southern Great Xing'an Range, China. *Acta Petrol. Sin.* **2017**, *33*, 3183–3199. (In Chinese with English abstract)
45. Chappell, B.W.; White, A.J.R. Two contrasting granite types. *Pacific Geol.* **1974**, *8*, 173–174.
46. Whalen, J.B.; Currie, K.L.; Chappell, B.W. A-type granites: Geochemical characteristics, discrimination and petrogenesis. *Contrib. Mineral. Petrol.* **1987**, *95*, 407–419. [CrossRef]
47. Petford, N.; Atherton, M. Na-rich partial melts from newly underplated basaltic crust: The Cordillera Blanca Batholith, Peru. *J. Petrol.* **1996**, *37*, 1491–1521. [CrossRef]
48. Li, X.H.; Li, W.X.; Li, Z.X. On the genetic classification and tectonic implications of the Early Yanshanian granitoids in the Nanling Range, South China. *Chin. Sci. Bull.* **2007**, *52*, 1873–1885. (In Chinese with English abstract) [CrossRef]
49. Beard, J.S.; Lofgren, G.E. Dehydration melting and water-saturated melting of basaltic and andesitic greenstones and amphibolites at 1, 3 and 6.9 kb. *J. Petrol.* **1991**, *32*, 365–401. [CrossRef]
50. Castro, A. Tonalite-granodiorite suites as cotectic systems: A review of experimental studies with applications to granitoid petrogenesis. *Earth Sci. Rev.* **2013**, *124*, 68–95. [CrossRef]
51. Kemp, A.I.S.; Hawkesworth, C.J.; Foster, G.L.; Paterson, B.A.; Woodhead, J.D.; Hergt, J.M.; Gray, C.M.; Whitehouse, M.J. Magmatic and crustal differentiation history of granitic rocks from Hf-O isotopes in zircon. *Science* **2007**, *315*, 980–983. [CrossRef]
52. Atherton, M.P.; Petford, N. Generation of sodium-rich magmas from newly underplated basaltic crust. *Nature* **1993**, *362*, 144–146. [CrossRef]
53. Deng, J.; Mo, X.; Zhao, H.; Luo, Z.; Zhao, G. Yanshanian magma–tectonic–metallogenic belt in east China of circum-Pacific domain (I): Igneous rocks, and orogenic processes. *J. China Univ. Geosci.* **1999**, *10*, 21–24. (In Chinese with English abstract)
54. Hofmann, A.W. Chemical differentiation of the Earth: The relationship between mantle, continental crust, and oceanic crust. *Earth Planet. Sci. Lett.* **1988**, *90*, 297–314. [CrossRef]
55. Green, T.H. Significance of Nb/Ta as an indicator of geochemical processes in the crust–mantle system. *Chem. Geol.* **1995**, *120*, 347–359. [CrossRef]
56. Taylor, S.R.; McLennan, S.M. *The Continental Crust: Its Composition and Evolution*; Blackwell Scientific Publications: Hoboken, NJ, USA, 1985; p. 312.
57. Rudnick, R.L.; Fountain, D.M. Nature and composition of the continental crust: A lower crustal perspective. *Rev. Geophys.* **1995**, *33*, 267–309. [CrossRef]
58. Li, W.B.; Huang, Z.L.; Xu, D.R.; Chen, J.; Xu, C.; Guan, T. Rb-Sr isotopic method on zinc–lead ore deposits: A review. *Geotect. Metall.* **2002**, *26*, 436–441. (In Chinese with English abstract)
59. Ma, X.H.; Chen, B.; Yang, M.C. Magma mixing origin for the Aolunhua porphyryrelated to Mo-Cu mineralization, eastern Central Asian Orogenic Belt. *Gondwana Res.* **2013**, *24*, 1152–1171. [CrossRef]
60. Jiang, S.H.; Liang, Q.L.; Liu, Y.F.; Liu, Y. Zircon U-Pb ages of the magmatic rocks occurring in and around the Dajing Cu-Ag-Sn polymetallic deposit of Inner Mongolia and constrains to the ore-forming age. *Acta Petrol. Sin.* **2012**, *28*, 495–513. (In Chinese with English abstract)
61. Wang, Y.; Fan, W.; Guo, F. K–Ar dating of late Mesozoic volcanism and geochemistry of volcanic gravels in the North Huaiyang Belt, Dabie orogen: Constraints on the stratigraphic framework and exhumation of the northern Dabie orthogneiss complex. *Chin. Sci. Bull.* **2002**, *47*, 1688–1695. [CrossRef]
62. Fan, W.M.; Guo, F.; Wang, Y.J.; Lin, G. Late Mesozoic calc-alkaline volcanism of post-orogenic extension in the northern Da Hinggan Mountains, northeastern China. *J. Volcanol. Geotherm. Res.* **2003**, *121*, 115–135. [CrossRef]
63. Zhou, J.B.; Wilde, S.A.; Zhang, X.Z.; Ren, S.M.; Zheng, C.Q. Early Paleozoic metamorphic rocks of the Erguna block in the Great Xing'an Range, NE China: Evidence for the timing of magmatic and metamorphic events and their tectonic implications. *Tectonophysics* **2011**, *499*, 105–117. [CrossRef]
64. Zhou, J.B.; Wilde, S.A.; Zhang, X.Z.; Zhao, G.C.; Zheng, C.Q.; Wang, Y.J.; Zhang, X.H. The onset of Pacific margin accretion in NE China: Evidence from the Heilongjiang high-pressure metamorphic belt. *Tectonophysics* **2009**, *478*, 230–246. [CrossRef]
65. Wang, T.; Zheng, Y.D.; Zhang, J.J.; Zeng, L.S.; Donskaya, T.; Guo, L.; Li, J.B. Pattern and kinematic polarity of late Mesozoic extension in continental NE Asia: Perspectives from metamorphic core complexes. *Tectonics* **2011**, *30*, 1–27. [CrossRef]
66. Liu, J.; Mao, J.W.; Wu, G.; Wang, F.; Luo, D.F.; Hu, Y.B. Zircon U-Pb and molybdenite Re-Os dating of the Chalukou porphyry Mo deposit in the northern Great Xing'an range, China and its geological significance. *J. Asian Earth Sci.* **2014**, *79*, 696–709. [CrossRef]
67. Hilde, T.W.C.; Uyeda, S.; Kroenke, L. Evolution of the western Pacific and its margin. *Tectonophysics* **1977**, *38*, 145–165. [CrossRef]

68. Wu, F.Y.; Lin, J.Q.; Wilde, S.A.; Zhang, X.O.; Yang, J.H. Nature and significance of the Early Cretaceous giant igneous event in eastern China. *Earth Planet. Sci. Lett.* **2005**, *233*, 103–119. [CrossRef]
69. Wang, F.; Zhou, X.H.; Zhang, L.C.; Ying, J.F.; Zhang, Y.T.; Wu, F.Y.; Zhu, R.X. Late Mesozoic volcanism in the Great Xing'an Range (NE China): Timing and implications for the dynamic setting of NE Asia. *Earth Planet. Sci. Lett.* **2006**, *251*, 179–198. [CrossRef]
70. Yu, J.J.; Wang, F.; Xu, W.L.; Gao, F.H.; Pei, F.P. Early Jurassic mafic magmatism in the Lesser Xing'an-Zhangguangcai Range, NE China, and its tectonic implications: Constraints from zircon U-Pb chronology and geochemistry. *Lithos* **2012**, *142*, 256–266. [CrossRef]
71. Zhang, F.Q.; Chen, H.L.; Yu, X.; Dong, C.W.; Yang, S.F.; Pang, Y.M.; Batt, G.E. Early Cretaceous volcanism in northern Songliao Basin, NE China, and its geodynamic implication. *Gondwana Res.* **2011**, *19*, 163–176. [CrossRef]
72. Xu, M.J.; Xu, W.L.; Meng, E.; Wang, F. LA–ICP–MS zircon U–Pb chronology and geochemistry of Mesozoic volcanic rocks from the Shanghulin–Xiangyang basins in Erguna area, and its tectonic implications. *Geol. Bull. China* **2011**, *30*, 1321–1338. (In Chinese with English abstract)
73. Wei, C.S.; Zhao, Z.F.; Spicuzza, M.J. Zircon oxygen isotopic constraint on the sources of late Mesozoic A-type granites in eastern China. *Chem. Geol.* **2008**, *250*, 1–15. [CrossRef]
74. Meng, F.C.; Liu, J.Q.; Cui, Y.; Gao, J.L.; Liu, X.; Tong, Y. Mesozoic tectonic regimes transition in the Northeast China: Constriants from temporal-spatial distribution and associations of volcanic rocks. *Acta Petrol. Sin.* **2014**, *30*, 3569–3586. (In Chinese with English abstract)
75. Wang, T.; Guo, L.; Zhang, L.; Yang, Q.D.; Zhang, J.J.; Tong, Y.; Ye, K. Timing and evolution of Jurassic-Cretaceous granitoid magmatisms in the Mongol-Okhotsk belt and adjacentareas, NE Asia: Implications for transition from contractional crustal thickening to extensional thinning and geodynamic settings. *J. Asian Earth Sci.* **2015**, *97*, 365–392. [CrossRef]
76. Han, S.J.; Wang, X.; Wang, X.; Wang, Y.; Zhang, Y. Geochronology and geochemistry of late Jurassic–Early Cretaceous volcanic rocks in the southern Great Xing'an range, NE China: Constraints for late Mesozoic tectono-magmatic evolution. *Int. Geol. Rev.* **2021**, *63*, 1366–1388. [CrossRef]
77. Wu, F.Y.; Sun, D.Y.; Li, H.M.; Jahn, B.M.; Wilde, S. A-type granites in northeastern China: Age and geochemical constraints on their petrogenesis. *Chem. Geol.* **2002**, *187*, 143–173. [CrossRef]
78. Zhang, L.Q.; Shao, J.A.; Zheng, G.R. Metamorphic core complex in Ganzhuermiao Inner Mongolia. *Sci. Geol. Sin.* **1998**, *33*, 14–20. (In Chinese with English abstract)
79. Zhang, X.D.; Yu, Q.; Chen, F.H.; Wang, X.W. Structural characteristics, origin and evolution of metamorphic core complex in central basement uplift and Xujiaweizi faulted depression in Songliao basin, Northeast China. *Earth Sci. Front.* **2000**, *7*, 411–419. (In Chinese with English abstract)
80. Liu, J.L.; Davis, G.A.; Lin, Z.Y.; Wu, F.Y. The Liaonan metamorphic core complex, southeastern Liaoning Province, North China: A likely contributor to Cretaceous rotation of eastern Liaoning, Korea and contiguous areas. *Tectonophysics* **2005**, *407*, 65–80. [CrossRef]
81. Shao, J.A.; Zhang, L.Q. Mesozoic dyke swarms in the north of North China. *Acta Petrol. Sin.* **2002**, *18*, 312–318. (In Chinese with English abstract)
82. Meng, E.; Xu, W.L.; Yang, D.B.; Qiu, K.F.; Li, C.H.; Zhu, H.T. Zircon U–Pb chronology, geochemistry of Mesozoic volcanic rocks from the Lingquan basin in Manzhouli area, and its tectonic implications. *Acta Petrol. Sin.* **2011**, *27*, 1209–1226. (In Chinese with English abstract)
83. Xu, W.L.; Pei, F.P.; Wang, F.; Meng, E.; Ji, W.Q.; Yang, D.B.; Wang, W. Spatial-temporal relationships of Mesozoic volcanic rocks in NE China: Constraints on tectonic overprinting and transformations between multiple tectonic regimes. *J. Asian Earth Sci.* **2013**, *74*, 167–193. [CrossRef]
84. Xu, W.L.; Wang, F.; Pei, F.P.; Meng, E.; Tang, J.; Xu, M.J.; Wang, W. Mesozoic tectonic regimes and regional ore-forming background in NE China: Constraints from spatial and temporal variations of Mesozoic volcanic rock associations. *Acta Petrol. Sin.* **2013**, *29*, 339–353.
85. Dong, Y.; Ge, W.C.; Yang, H.; Zhao, G.C.; Wang, Q.H.; Zhang, Y.L.; Su, L. Geochronology and geochemistry of Early Cretaceous volcanic rocks from the Baiyingaolao formation in the central Great Xing'an range, NE China, and its tectonic implications. *Lithos* **2014**, *205*, 168–184. [CrossRef]
86. Yu, Y.; Xu, W.L.; Pei, F.P.; Yang, D.B.; Zhao, Q.G. Chronology and geochemistry of Mesozoic volcanic rocks in the Linjiang area, Jilin Province and their tectonic implications. *Acta Geol. Sin.* **2009**, *83*, 245–257. [CrossRef]
87. Zhu, R.X.; Xu, Y.G. The subduction of the west Pacific plate and the destruction of the North China Craton. *Sci. China Earth Sci.* **2019**, *49*, 1340–1350. (In Chinese with English abstract) [CrossRef]
88. Liu, J.L.; Ni, J.L.; Chen, X.Y.; Craddock, J.P.; Zheng, Y.Y.; Ji, L.; Hou, C.R. Early Cretaceous tectonics across the North Pacific: New insights from multiphase tectonic extension in Eastern Eurasia. *Earth Sci. Rev.* **2021**, *217*, 103552. [CrossRef]
89. Tang, J.; Xu, W.L.; Wang, F.; Ge, W.C. Subduction history of the Paleo-Pacific slab beneath Eurasian continent: Mesozoic-Paleogene magmatic records in Northeast Asia. *Sci. China Earth Sci.* **2018**, *61*, 527–559. (In Chinese with English abstract) [CrossRef]
90. Zhu, X.; Chen, H.J.; Sun, Z.C.; Zhang, Y.C. The Mesozoic-Cenozoic tectonics and petroliferous basins of China. *Acta Geol. Sin.* **1983**, *3*, 235–242. (In Chinese with English abstract)

91. Tian, Y.; Ma, J.C.; Liu, C.; Feng, Y.; Liu, T.T.; Zhu, H.X.; Yan, D.; Li, H.H. Effects of subduction of the western Pacific plate on tectonic evolution of Northeast China and geodynamic implications. *Chin. J. Geophys.* **2019**, *62*, 1071–1082. (In Chinese with English abstract)
92. Pearce, J.A.; Harris, N.B.W.; Tindle, A.G. Trace element discrimination diagrams for the tectonic interpretation of granitic rocks. *J. Petrol.* **1984**, *25*, 956–983. [CrossRef]
93. Harris, N.B.; Pearce, J.A.; Tindle, A.G. Geochemical characteristics of collision-zone magmatism. In *Collision Tectonics*; Coward, M.P., Reis, A.C., Eds.; Geological Society of London: London, UK, 1986; pp. 67–81.
94. Luchitskaya, M.V.; Morozov, O.L.; Palandzhyan, S.A. Plagiogranite magmatism in the Mesozoic island-arc structure of the Pekulney Ridge, Chukotka Peninsula, NE Russia. *Lithos* **2004**, *79*, 251–269. [CrossRef]